ChemCatChem

Research Article
doi.org/10.1002/cctc.202200345

Chemistry Europe
European Chemical Societies Publishing

www.chemcatchem.org

Special Collection

Fluxionality of Subnano Clusters Reshapes the Activity Volcano of Electrocatalysis

Zisheng Zhang,[a] Borna Zandkarimi,[a] Julen Munarriz,[a, b] Claire E. Dickerson,[a] and Anastassia N. Alexandrova*[a, c]

The Sabatier activity volcano provides intuitive guide for catalyst design, but also imposes fundamental limitations on the composition and maximal activity of catalysts. We show that the ORR activity volcano is shifted and reshaped by the potential-dependent fluxionality of subnano cluster catalysts. Fluxionality causes the typically under-binding Ag/Au to gain optimal activity in the cluster form, and surpass Pt/Pd. Furthermore, isomerization of clusters as a function of the potential breaks linear scaling relationships, enabling surpassing the volcano "apex" relative to the bulk. The effect is likely general for fluxional cluster catalysts.

Introduction

Activity volcano, based on the Sabatier principle and the scaling relationships of adsorption energetics, has been a time-tested model for catalyst design in heterogeneous thermal and electrocatalysis.[1,2] It states that the catalyst with maximal activity should have an intermediate and optimal binding strength with reactants, or else the activation or product desorption step will become rate-limiting due to under- or over-binding. Although the activity volcano model provides a simple and intuitive picture for optimizing catalysts, it poses an intrinsic limitation on the maximal activity for a given reaction.[3]

Subnano clusters have been demonstrated to have not only higher atomic efficiency but also fluxionality that set them apart from their bulk counterparts.[4] Their relatively flat potential energy surface (PES) make them exceptionally dynamic. At finite temperatures, clusters can visit the low-energy local minima, populating a pool of isomers with distinct structures and reactivities, best represented as a statistical ensemble.[5] In addition, subnano clusters can adapt their shapes and binding sites to bind different adsorbates, causing a breakdown of the scaling relationships (which normally assume consistent binding modes among chemically similar adsorbates), and even potential non-Arrhenius behavior of reaction kinetics.[6,7]

The oxygen reduction reaction (ORR) is a well-studied electrocatalytic reaction where a robust scaling relationship and an activity volcano are observed for bulk metal surfaces.[8] Since the scaling relationships underly the regular shape of the ORR activity volcano, we expect the fluxionality of subnano clusters to undermine the volcano. In addition, we show that fluxionality is strongly dependent on the applied electrochemical potential, further distorting the portrait of the catalyst and the volcano. Overall, dynamic restructuring pushes typically under-binding elements to, and in some cases beyond the ORR volcano top. The phenomenon is expected to be generalizable to other dynamic catalysts, opening a new dimension in catalyst design.

Results and Discussion

For the ORR, we consider the 4-electron dissociative and associative pathways which involve *O, *OH, and *OOH intermediates (* represents the catalyst's active site). The calculated binding energies ΔE_O, ΔE_{OH}, and ΔE_{OOH} are referenced against the energies of H_2O and H_2 by corresponding stoichiometries. For the (111) surfaces of bulk metals, the binding energy of the three adsorbates correlate, and E_O is often used to estimate the binding energies of other adsorbates and activation barriers.[8]

In this work we focus on Pd, Pt, Ag, and Au, a set that includes the two most active elements on both arms of the ORR activity volcano for bulk (111) surfaces.[8] First, we study the subnano clusters M_n (M=Pd, Pt, Ag, Au; n = 1–6) in the isolated form. A statistical ensemble of isomers is constructed for each bare and adsorbate-bound cluster via global optimization with bond length distribution algorithm (BLDA).[9] The adsorbate binding energies are calculated using ensemble-average ener-

[a] Z. Zhang, Dr. B. Zandkarimi, Prof. J. Munarriz, C. E. Dickerson, Prof. A. N. Alexandrova
Department of Chemistry and Biochemistry
University of California, Los Angeles
607 Charles E. Young Drive
Los Angeles, CA 90095–1569 (USA)
E-mail: ana@chem.ucla.edu
Homepage: http://www.chem.ucla.edu/~ana/
[b] Prof. J. Munarriz
Departamento de Química Física y Analítica
Universidad de Oviedo
Julián Clavería n° 8, Campus Universitario de El Cristo
Oviedo, 33006 (Spain)
[c] Prof. A. N. Alexandrova
California NanoSystem Institute
University of California, Los Angeles
607 Charles E. Young Drive
Los Angeles, CA 90095–1569 (USA)

Supporting information for this article is available on the WWW under https://doi.org/10.1002/cctc.202200345

Special Collection *This publication is part of a joint Special Collection with ChemElectroChem on "Catalysts and Reactors under Dynamic Conditions for Energy Storage and Conversion (DynaKat)". Please check ourhomepage for more articles in the collection.*

gies by Boltzmann populations at 300 K corresponding to the room temperature fuel cells.[10]

First, the isolated clusters have an overall stronger binding of O, by 0.5–2.0 eV compared to the bulk surfaces (Figure 1a). The binding strengthening originates from the undercoordination of atoms in clusters, as well as fluxionality enabling them to rearrange in response of adsorbates thus maximizing the binding. As a result, ΔE_O of Au_n and Ag_n clusters strengthen to around 1.5 eV, which is close to the ΔE_O of bulk Pt(111) and Pd(111), suggesting new winners in ORR catalysis. Pt_n and Pd_n, become over-binding. The ORR activity of M_n was calculated using an adapted microkinetic model from ref: [8]

$$A = k_B T \min_i[\log(k_i/k_0)];\ k_i = \nu_i \exp(\Delta G_i/k_B T)$$

Where the pre-factors are taken from ref. 8, and energies are the computed thermal ensemble-averages. We find (Figure 1b) the activity of some Au_n/Ag_n, such as Ag_2 and Au_6, to be comparable to that of Pd(111), whereas the activity of Pd_n and Pt_n to fall below those of Ag(111) and Au(111), respectively. Notably, there is no monotonic relation between cluster size and activity, nor is there a consistent trend among different metals, reinforcing the concept of "each atom counts".[11,12]

The correlation between ΔE_{OH} and ΔE_O for bulk(111) and isolated cluster forms is shown in Figure 1c, again illustrating how selected Ag and Au clusters land the closest to the best bulk ORR catalysts, Pt(111) and Pd(111). We also see how the linear scaling relationship breaks down for subnano clusters with a poor $R^2 = 0.60$ (versus $R^2 = 0.91$ for bulk surfaces), due to adsorbate-dependent cluster isomerization.[6]

Compared to their bulk(111) values, the energies of isolated clusters shift toward the lower left region due to strengthening of O and OH binding. The shift is larger for ΔE_{OH} likely due to change in adsorbate configuration: O adsorbs majorly at bridge site both on bulk (111) and on clusters, whereas OH majorly adsorbs at atop site on bulk (111) but at bridge site on clusters.

This exploration qualitatively informs about the direction of the volcano reshaping for clusters. However, it can be expected that the deposition onto the cathode in a practical device would further strongly impact cluster catalysts. Clearly, the intra-cluster chemical bonding (and hence, the structure, nature of the active sites, and reactivity) should be very sensitive to the change of electron count. However, to the best of our knowledge, no theoretical work to date addresses these effects of the potential (i.e., actual electrode charging). We study M_4 supported on carbon (denoted as M_4/C) in the presence of the applied potential. The tetramer is chosen for its significant fluxionality, relatively small configurational space, and well-defined core shapes (Figure 2a). The carbon substrate is modeled by a graphite slab (see section, Methods), which could represent the surface of glassy carbon electrode or any graphitic carbon substrate.[13,14]

First, the ensemble-averaged cluster-support interaction energies in the absence of the applied potential are calculated to be −1.92 eV, −1.30 eV, −1.03 eV, and −0.64 eV for Pd, Pt, Ag, and Au, respectively. The strongest cluster-support binding for Pt_4/C flips its isomer distribution at 300 K: from the butterfly structure being prevalent over the tetrahedral in the gas phase, to the tetrahedron being prevalent over the butterfly on the surface. For the other three metals, the distribution is almost unchanged between isolated and supported forms (Figure S1). M_4/C systems feature stronger binding of the adsorbates compared to their bulk (111), but the shifts are, expectedly, smaller compared to isolated clusters (Figure 1d). The shift

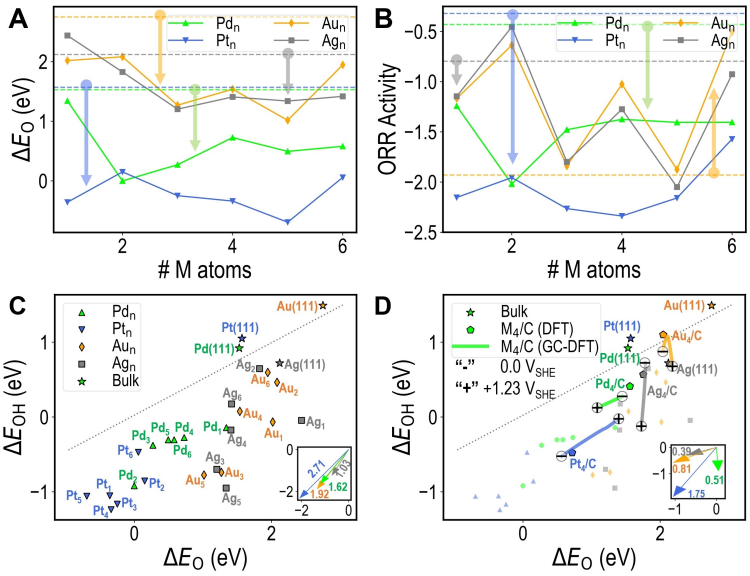

Figure 1. ORR energetics of isolated and graphite-supported clusters. (A) Binding energy for *O and (B) ORR activity of gas phase Pd_n, Pt_n, Au_n, Ag_n clusters with n = 1–6. Values of bulk (111) surfaces are shown in dashed lines. The distribution of *OH and *O binding energies of (C) isolated and (D) graphite-supported clusters. The scaling relationship for bulk (111) is shown as dotted lines. "+" and "−" label the 0 V_{SHE} and 1.23 V_{SHE} values in the GCDFT curve. Insets show the shift from bulk (111) values to $M_{1\text{-}6}$ values (averaged for each element, in C) and M_4/C values (in D). All ORR activities are in unit k_BT.

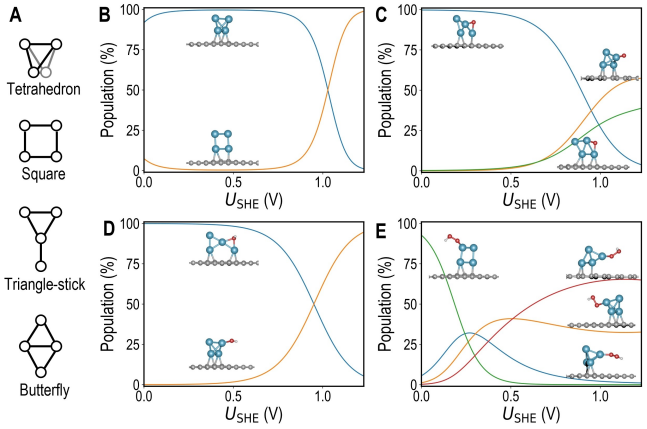

Figure 2. Potential-dependent isomer distributions (core shapes summarized in a) of (b) *, (c) *O, (d) *OH, and (e) *OOH intermediates on Pt_4/C at 300 K. Each curve represents an isomer, and the corresponding geometry is labeled next to it.

directions diverge for different M_4/C systems (Figure 1d inset), attributable to the competition between intra-cluster, cluster-support, and cluster-adsorbate interactions. For example, for Pt, the change of the global minimum (GM) is due to the cluster-support interaction outcompeting the intra-cluster metal-metal interactions. The competition among different interactions can also be observed in the pair-correlation heatmap in Figure S2 – intuitively placing properties of clusters between those of the bulk and isolated atoms. For example, ΔE_O of bulk (111) correlates with the Brinell hardness, which is an empirical measure of the bulk property. However, ΔE_O of clusters correlates better with atomic-related properties such as bond dissociation energy of the M–O dimer, cohesive energy of the bulk, and ionization energy (Figure S2).

At a realistic electrochemical interface, the binding energy of adsorbate is potential-dependent and configuration-specific.[15,16] Here, we additionally see that the electrode potential can significantly affect the populations of cluster isomers in the ensemble even at room temperature (Figures 2b, S4–S6). For example, for Pt_4/C, the isomer distribution for each ORR intermediate (Boltzmann statistics at 300 K), calculated from grand canonical DFT (GCDFT) electronic free energies changes significantly as a function of U (Figure 2). For the bare Pt_4/C at low overpotential, the square configuration is favored, but as the potential sweeps across c.a. 1.0 V in the SHE scale, the tetrahedron configuration becomes dominant (Figure 2b). For the *O intermediate (Figure 2c), however, the square is inaccessible, and instead the tetrahedron, butterfly, and triangle-stick coexist at low overpotential. At higher overpotential, the triangle-stick becomes dominant. For the *OH intermediate (Figure 2d), the butterfly is inaccessible, and the low and high overpotential regions are dominated by tetrahedron and triangle-stick, respectively. For *OOH (Figure 2e), the potential-dependent ensemble gets more complicated, with the butterfly, tetrahedron, and square dominating the low, medium, and high overpotentials, respectively. The analyses for Pd, Au, and Ag are given in Figures S4–S6.

The complexity brought about by the potential dependence originates in the different potential sensitivity of each isomer for each M. The electronic free energy-potential relation here is approximated by a capacitance model with parabolic shape where the location of the maximum corresponds to the isomer-specific potential of zero charge (PZC), and the curvature indicates the polarizability of the system (Figure S3).[17] As these two properties vary among cluster isomers, the parabolic functions and isomer populations exhibit crossovers. The isomers can differ by: (i) configuration of the metal core, (ii) adsorbate configurations (orientation and bonding mode), and (iii) cluster-support interaction. For example, although the core structure of Pd_4/C remains tetrahedral for all reaction intermediates (Figure S4), the cluster-surface interaction (Figure S4a) and adsorbate configurations (Figure S4b) diversify the ensemble. There are also cases where a specific isomer dominates in the whole ORR potential window, such as Pd_4*OH/C (Figure S4c), Pd_4*OOH/C (Figure S4d), Ag_4*O/C (Figure S5b), and Au_4/C (Figure S6a), and cases where multiple isomers coexist in a wide potential range, such as Pt_4*OOH/C (Figure 2e), Au_4*OH/C (Figure S6c). Note that we assume the fully Boltzmann ensemble, i.e., that barriers of cluster isomerization are small and easily crossed in reaction conditions (discussions in Supplementary Note 2).[18] The ensemble size is determined by the architecture of the potential-dependent free energy surface, which cannot be expressed in a unified model based on simple elemental properties, nor predicted without performing global optimization for every reaction intermediate in the presence of electrode potential (see Methods). We note that the associated computational expense is truly formidable, compared to the customarily adopted CHE model. The ensemble-averaged $\Delta E_O - \Delta E_{OH}$ in the potential range of 0 to 1.23 V_{SHE} can shift away from the constant-charge DFT results by as much as 1 eV, and the shifting direction is metal-dependent (Figure 1d).

The free energy change of each ORR step, $\Delta G_i(U)$ (i=1–4), following the associative 4-electron pathway: (1) $*+O_2+H^++e^-==*OOH$, (2) $*OOH+H^++e^-==*O+H_2O$, (3) $*O+H^++e^-==*OH$, (4) $*OH+H^++e^-==*+H_2O$, in the potential range of 0 to 1.23 V_{SHE}, do not follow the usually assumed linear potential-dependence of 1 eV per V[19] (Figure 3). In fact, most of them are not linear, with each curve bending corresponding to an isomer population crossover in Figure 2. The step 4 (*OH desorption, red curve) becomes the potential-determining step (PDS) of the reaction for all M_4/C systems except for Au_4/C. Au and Ag, which have difficulty activating O_2 as bulk (111), now have much more favorable ΔG_1. As a result, the onset potential (potential at which all ΔG_i become negative) for Ag_4/C and Au_4/C shifted to much more positive, thanks to the strengthening of *OOH binding. However, Pd_4/C and Pt_4/C suffer from severe *OH over-binding (step 4), and the expected onset potentials are much more negative compared to those of Au_4/C and Ag_4/C.

The found effects reshape the ORR volcano as follows. While for the bulk (111), Pt and Pd are near the apex, and Ag and Au are far below on the right arm (Figure 4a), for isolated clusters

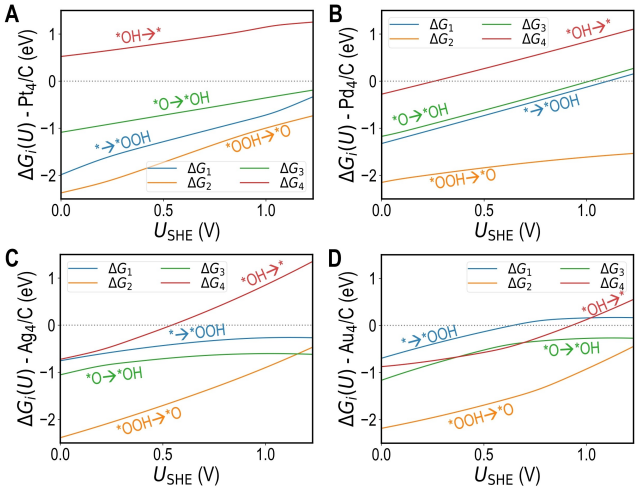

Figure 3. The potential-dependent reaction free energies of steps 1–4 of the 4-e associative ORR pathway for (a) Pt_4/C, (b) Pd_4/C, (c) Ag_4/C, and (d) Au_4/C. A simplified chemical equation for each step is labeled along each curve.

(Figure 4b), the strengthening of binding causes a pronounced shift bringing Ag and Au to the apex, and Pt and Pd – down to the left. In addition, the fluxionality of clusters breaks the linear scaling relationships and thus roughen the volcano landscape. Finally, for graphite-supported M_4 (Figure 4c), the left-ward shifting qualitatively persists. When the electrode potential is included, the potential-dependent isomer distribution opens an additional dimension affecting the ORR activity, enabling the supported subnano clusters to go beyond the volcano top at certain electrode potentials. The volcano shape that varies with applied potential is similar to the LSR-based analysis in ref [20] but is of a different origin: a potential dependent statistical ensemble representation of the supported subnano cluster. Note that the ORR activity in this study is calculated using kinetics prefactor fitted to experiments on bulk(111),[8] whereas the isolated and supported subnano clusters would have a higher density of active sites and electrochemical active surface area, at a similar or lower metal loading.[21] Therefore, we would expect the measured ORR activity (current density at a given overpotential) to be significantly higher for subnano clusters than for single crystal surfaces or nanoparticles, despite a similar calculated ORR activity.

The potential dependent part of the total reaction free energy due to isomerization for other cluster sizes is not investigated herein, but we would expect a non-consistent trend (similar to Figure 1A–B) where the potential dependence goes for some sizes while against the others. Hence, although the activity of Ag_4/C drops to around that of Pd_4/C or Pt_4/C at a practical potential range, we still regard it as a promising candidate element due to a higher "baseline" activity. Further maximizing the ORR activity beyond Au_4/C might be possible via: (i) alloying two (or more) metals on two sides of the activity volcano, (ii) heteroatom doping of nonmetal or semimetal elements, or (iii) introducing lanthanides or actinides which are located on the weak-binding side of the activity volcano due to relativistic effects.[22]

Sintering of single atoms and small clusters has been observed after electrochemical cycling,[23,24] and this poses a challenge to the long-term cluster electrocatalyst stability, especially when binding to the support is weaker, as for Ag and Au (Figures S5c–d, S6c). One approach to mitigate sintering is to use a conductive substrate with appropriate anchoring sites, such as graphdiyne, black phosphorous, nanocarbon with engineered defects (reduced graphene oxide, heteroatom-doped graphene etc.), and conducting metal oxides.[25–27] While stronger cluster-support interaction will reshape the PES of the cluster and affect the cluster-support charge transfer,[28–30] we expect the trends across fluxional clusters toward increased activity of more weakly binding metals to hold true.

In this study, to compare with the reported adsorbate binding energies on bulk (111) at $^1/_4$ monolayer coverage, we only consider one adsorbate on the M_4/C systems. However, at higher current density and reagent concentration, the coverage may increase; the binding energy and site of the second and subsequent adsorbates will depend on the previous adsorbates,[5] yielding an exponentially growing number of possible configurations. Some adsorbates may remain bound to the cluster throughout the catalysis, effectively altering the catalyst stoichiometry. However, we expect the fluxionality to persist even under stoichiometric changes, enabling the clusters

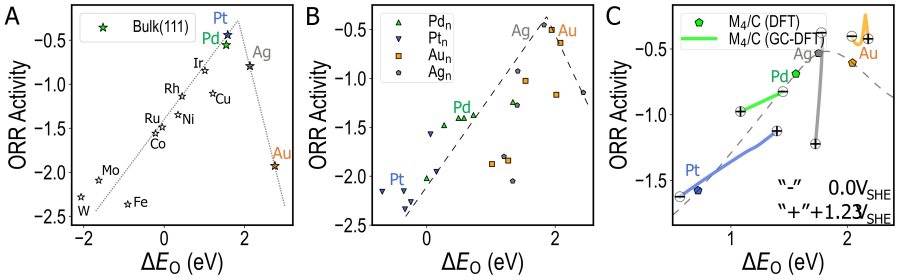

Figure 4. The ORR activity volcano for (a) bulk (111), (b) isolated $M_{1\text{-}6}$ clusters, and (c) M_4/C. "+" and "−" mark the 0 V_{SHE} and 1.23 V_{SHE} values in the GCDFT curve. The qU term is subtracted from GCDFT energetics when calculating the activity in (c) to show the non-CHE part of the potential-dependence. Dotted and dash-dot curves are analytical volcano for bulk (111) in ref [8] and putative volcano for subnano clusters in this study, respectively. All ORR activities are in unit k_BT.

to maintain reagent over-binding, since the cluster cat always reshape to gain in intra-cluster bonding if the binding to the new adsorbate is too weak (we currently investigate this effect). Hence, the shifting compared to bulk surfaces should hold.

Conclusion

In summary, we show that the apex of the electrocatalytic ORR activity volcano shifts from Pd/Pt to Ag/Au in the regime of subnano clusters due to their adsorbate-, potential-, and metal-dependent restructuring (specific fluxionality) in reaction conditions. Fluxionality breaks the linear scaling relationship, and overall strengthens the adsorbate binding energies, making O_2 activation no longer a barrier for Ag/Au while giving Pt/Pd a severe over-binding problem. We show for the first time that the change in electrode potential within the ORR potential window can alter the cluster isomer distribution, making the relationship between reaction free energies and electrode potential highly non-linear, enabling surpassing the bulk volcano apex. Overall, we expect cluster fluxionality to generally shift the volcano for cluster catalysis to the left, making under-binding elements more catalytic. In other words, fluxionality – the very curse complicating cluster catalysis – can be used strategically in cluster catalysis design.

Experimental Section

The isolated subnano clusters are modeled in a large unit cell of 20 Å×20 Å×20 Å. The graphite substrate is modeled by a (6×6×3) graphite slab, with the bottom two layers constrained to represent bulk behavior and a vacuum slab of 25 Å thickness. The isomer and adsorbate configurations in both isolated and supported forms are sampled using the bond length distribution algorithm (BLDA) as implement in our open source Python package, PGOPT. The local optimization and energy evaluation of the generated structures are performed with the PBE functional[31] and PAW pseudopotentials[32] using the VASP program (version 5.4.1).[33–36] DDsC correction is used to account for the dispersion interactions.[37] Implicit solvation model (solvent: water) is used for all calculations using the linearized Poisson-Boltzmann model[38] (with a Debye length of 3 Å) as implemented in the VASPsol code.[39] Spin polarization is turned on throughout the global optimization sampling process, and the multiplicity (which has been reported to make little difference on energetics[9]) is considered to be sampled as sufficiently as the geometry. Due to the relatively large system and sampling size, only the Γ *k*-point is sampled in the reciprocal space of the Brillouin zone, and the cutoff energy for the kinetic energy of the plane-waves was 400 eV. The convergence criteria are set to 10^{-6} eV for SCF iteration and 0.05 eV/Å for the forces. The grand canonical DFT calculations employ the surface charging technique reported in ref. [17] using a symmetrized slab with a 25 Å vacuum gap. The adsorbate binding energies, reaction free energies, and ORR activity are calculated using the expressions in ref. [8] but the energies are from ensemble average instead of the linear scaling relationships.

Acknowledgements

We acknowledge the support from the U.S. Department of Energy grant DE-SC0020125, and the computational resources at NERSC and UCLA shared cluster, Hoffman2.

Conflict of Interest

The authors declare no conflict of interest.

Data Availability Statement

The data that support the findings of this study are available from the corresponding author upon reasonable request.

Keywords: Cluster catalysis · Electrochemistry · Fluxionality · Oxygen reduction reaction · Sabatier principle

[1] T. Bligaard, J. K. Nørskov, S. Dahl, J. Matthiesen, C. H. Christensen, J. Sehested, *J. Catal.* **2004**, *224*, 206–217.
[2] H. Ooka, J. Huang, K. S. Exner, *Front. Energy Res.* **2021**, *9*, 155.
[3] Z.-F. Huang, J. Song, S. Dou, X. Li, J. Wang, X. Wang, *Matter* **2019**, *1*, 1494–1518.
[4] H. Zhai, A. N. Alexandrova, *ACS Catal.* **2017**, *7*, 1905–1911.
[5] Z. Zhang, B. Zandkarimi, A. N. Alexandrova, *Acc. Chem. Res.* **2020**, *53*, 447–458.
[6] B. Zandkarimi, A. N. Alexandrova, *J. Phys. Chem. Lett.* **2019**, *10*, 460–467.
[7] B. Zandkarimi, A. N. Alexandrova, *J. Phys. Chem. C* **2020**, *124*, 19556–19562.
[8] J. K. Nørskov, J. Rossmeisl, A. Logadottir, L. Lindqvist, J. R. Kitchin, T. Bligaard, H. Jónsson, *J. Phys. Chem. B* **2004**, *108*, 17886–17892.
[9] H. Zhai, A. N. Alexandrova, *J. Chem. Theory Comput.* **2016**, *12*, 6213–6226.
[10] N. R. Markovic, P. N. Ross, *CATTECH* **2000**, *4*, 110–126.
[11] M. Valden, X. Lai, D. W. Goodman, *Science* **1998**, *281*, 1647–1650.
[12] U. Heiz, A. Sanchez, S. Abbet, W.-D. Schneider, *J. Am. Chem. Soc.* **1999**, *121*, 3214–3217.
[13] H. Tsunoyama, A. Ohnuma, K. Takahashi, A. Velloth, M. Ehara, N. Ichikuni, M. Tabuchi, A. Nakajima, *Chem. Commun.* **2019**, *55*, 12603–12606.
[14] A. Ohnuma, K. Takahashi, H. Tsunoyama, T. Inoue, P. Zhao, A. Velloth, M. Ehara, N. Ichikuni, M. Tabuchi, A. Nakajima, *Catal. Sci. Technol.* **2022**, *12*, 1400–1407 .
[15] S. N. Steinmann, P. Sautet, *J. Phys. Chem. C* **2016**, *120*, 5619–5623.
[16] S. N. Steinmann, C. Michel, R. Schwiedernoch, J. Filhol, P. Sautet, *ChemPhysChem* **2015**, *16*, 2307–2311.
[17] S. N. Steinmann, C. Michel, R. Schwiedernoch, P. Sautet, *Phys. Chem. Chem. Phys.* **2015**, *17*, 13949–13963.
[18] T. Imaoka, T. Toyonaga, M. Morita, N. Haruta, K. Yamamoto, *Chem. Commun.* **2019**, *55*, 4753–4756.
[19] D. R. Alfonso, D. N. Tafen, D. R. Kauffmann, *Catalysts* **2018**, *8*, 424.
[20] K. S. Exner, *J. Phys. Chem. C* **2019**, *123*, 16921–16928.
[21] Z. Tang, W. Wu, K. Wang, *Catalysts* **2018**, *8*, 65.
[22] W. Feng, H. Chen, Q. Zhang, R. Gao, X. Zou, *Chin. J. Catal.* **2020**, *41*, 1692–1697.
[23] Z. Weng, Y. Wu, M. Wang, J. Jiang, K. Yang, S. Huo, X. F. Wang, Q. Ma, G. W. Brudvig, V. S. Batista, Y. Liang, Z. Feng, H. Wang, *Nat. Commun.* **2018**, *9*, 1–9.
[24] A. Corma, P. Concepción, M. Boronat, M. J. Sabater, J. Navas, M. J. Yacaman, E. Larios, A. Posadas, M. A. López-Quintela, D. Buceta, *Nat. Chem.* **2013**, *5*, 775–781.
[25] J.-C. Liu, H. Xiao, J. Li, *J. Am. Chem. Soc.* **2020**, *142*, 3375–3383.
[26] X. Chia, M. Pumera, *Nat. Catal.* **2018**, *1*, 909–921.
[27] A. von Weber, E. T. Baxter, S. Proch, M. D. Kane, M. Rosenfelder, H. S. White, S. L. Anderson, *Phys. Chem. Chem. Phys.* **2015**, *17*, 17601–17610.

[28] E. Jimenez-Izal, H. Zhai, J.-Y. Liu, A. N. Alexandrova, *ACS Catal.* **2018**, *8*, 8346–8356.
[29] H. Zhai, A. N. Alexandrova, *J. Phys. Chem. Lett.* **2018**, *9*, 1696–1702.
[30] E. T. Baxter, M.-A. Ha, A. C. Cass, H. Zhai, A. N. Alexandrova, S. L. Anderson, *J. Phys. Chem. C* **2018**, *122*, 1631–1644.
[31] C. Adamo, V. Barone, *J. Chem. Phys.* **1999**, *110*, 6158–6170.
[32] G. Kresse, D. Joubert, *Phys. Rev. B* **1999**, *59*, 1758.
[33] G. Kresse, J. Furthmüller, *Comput. Mater. Sci.* **1996**, *6*, 15–50.
[34] G. Kresse, J. Furthmüller, *Phys. Rev. B* **1996**, *54*, 11169–11186.
[35] G. Kresse, J. Hafner, *Phys. Rev. B* **1993**, *47*, 558.
[36] G. Kresse, J. Hafner, *Phys. Rev. B* **1994**, *49*, 14251.
[37] S. N. Steinmann, C. Corminboeuf, *J. Chem. Phys.* **2011**, *134*, 44117.
[38] K. Mathew, V. S. C. Kolluru, S. Mula, S. N. Steinmann, R. G. Hennig, *J. Chem. Phys.* **2019**, *151*, 234101.
[39] K. Mathew, R. Sundararaman, K. Letchworth-Weaver, T. A. Arias, R. G. Hennig, *J. Chem. Phys.* **2014**, *140*, 84106.

Manuscript received: March 9, 2022
Revised manuscript received: May 17, 2022
Accepted manuscript online: May 20, 2022
Version of record online: ■■, ■■■

RESEARCH ARTICLE

Up in the mountains: ORR activity volcano is shifted and reshaped by the potential-dependent fluxionality of subnano cluster catalysts, bringing inert Ag/Au to the apex. Furthermore, isomerization of clusters as a function of the potential breaks linear scaling relationships, enabling surpassing the volcano "apex" relative to the bulk.

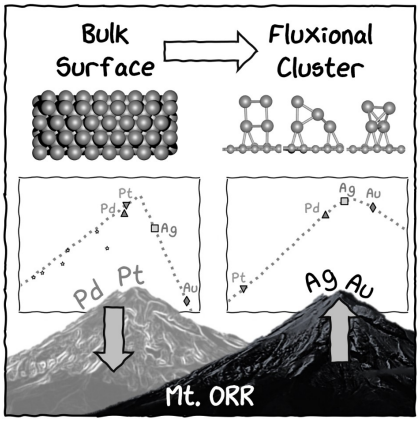

*Z. Zhang, Dr. B. Zandkarimi, Prof. J. Munarriz, C. E. Dickerson, Prof. A. N. Alexandrova**